文章编号：1001－9014(2015)06－0710－06
DOI:10.11972/j.issn.1001－9014.2015.06.014

Space projection estimator and temporal iteration scene-based non-uniformity correction algorithm

XU Hong-Lie, CHEN Qian, SUI Xiu-Bao, REN Jian-Le, REN Kan

(1. Jiangsu Key Laboratory of Spectral Imaging & Intelligence Sense, Nanjing University of Science and Technology, Nanjing 210094, China;
2. Taihu University of Wuxi, Wuxi 214064, China)

Abstract: In this paper, an improved scene-based non-uniformity correction (SBNUC) algorithm called space projection estimator and temporal iteration (SPETI) is proposed. This method estimates the global translation by the projection estimator and iterates between several adjacent frames. The detailed method includes three main steps. First, we develop a new projection estimator for the registration with a criterion. Then, correlation of adjacent frames, together with iteration strategy between them, is used in order to get fast and reliable fixed-pattern noise (FPN) reduction with low few ghosting artifacts. Finally, this algorithm is immigrated into an FPGA-based hardware system. We test the performance of our algorithm by the evaluation indexes, and demonstrate the actual effect of correcting the non-uniformity under a monotonous motion on the system. In order to compare with the gated adaptive least mean square (GALMS) method and the total variation (TV) method, a clean infrared image sequences with synthetic non-uniformity is studied. Normal distributed gain and offset non-uniformity are applied to the image sequences to study the relationship of iteration times and level of non-uniformity.

Key words: scene-based non-uniformity correction, space projection estimator, temporal iteration, continuous monotonous motion, FPGA
PACS: 42.30.-d

基于场景的空间投影估计和时域迭代非均匀性校正算法

许轰烈, 陈 钱, 隋修宝, 任建乐, 任 侃
(1. 南京理工大学 江苏省光谱成像与智能感知重点实验室,江苏 南京 210094;
2. 无锡太湖学院,江苏 无锡 214064)

摘要:提出了一种基于场景的空间投影估计和时域迭代百均匀性校正算法(SPETI).这种方法 主要是通过投影估计来估算全局位移,并且在连续多帧图像中进行迭代计算.首先,为配准准则设计了一个新的投影估计;然后,计算相邻帧并进行迭代计算,以此来获得较快的固定图案噪声(FPN)收敛,同时减少鬼影的产生;最后,将本算法移植至基于FPGA的硬件系统中.在连续单调运动的系统中测试算法的各项指标,并且将实际的校正效果予以展示.为了与自适应最小均方差算法和全变差算法进行比较,对一个完全干净的红外图像序列添加了人为的非均匀性.将固定标准增益和偏置非均匀性添加到图像序列上,以测试迭代次数与非均匀性等级的关系.

关 键 词:基于场景的非均匀性校正;空间投影估计;时域迭代;连续单调运动;FPGA
中图分类号:TN219 **文献标识码**:A

Introduction

Infrared focal plane array (IRFPA) sensors are widely used in the fields of aviation, industry, agriculture, medicine and scientific research. However, because of the disparity of technology equipment and the defect of material, IRFPA has an intrinsic shortcoming that is the non-uniformity which results in a fixed pattern noise on images[1]. In order to solve the problem, corre-

Received date: 2014-12-07, **revised date**: 2015-10-16 **收稿日期**:2014-12-07, **修回日期**:2015-10-16
Foundation items:Supported by the Natural Science Foundation of Jiangsu Province of China(BK20130769)
Biography:XU Hong-Lie(1986-), male, Wuxi, Jiangsu Province, Ph. D. Research area involves image processing. E-mail: sangxing1988@163.com

sponding non-uniformity correction (NUC) algorithms have been proposed, especially the scene based non-uniformity algorithms. The scene based non-uniformity algorithms have been developed rapidly nowadays, such as the constant statistical NUC[2-8] algorithm, the neural network NUC algorithm[9-13], the image registration NUC algorithm[14-16], and the time-domain high-pass filter NUC algorithm[17-20]. All the algorithms mentioned above have their scope of application. For example, the high-pass filter NUC algorithm, neural network NUC algorithm and the constant statistical NUC algorithm perform well on the high space frequency non-uniformity[5,9,11,18-19], but incredibly poorly towards the low space frequency non-uniformity, and even worse, the ghost artifacts when the scene is from rest to movement[6-7,10,20-21]. The registration NUC algorithm performs well on these two kinds of non-uniformity[13-15], but it cannot avoid facing the fatal problem of the possible misregistration, which can cause the error correction. Until today, the research of most scene-based NU correction algorithms is remaining in the laboratory stage. They may be developed very sophisticated, but no report shows that they can be realized on the small packaged, low power consumed real time hardware systems. Meanwhile, most video sequences captured for testing the performance of an algorithm are under good state of motion, which means that the scene motion is enough in all directions. However, in real application, most scenes have both the high frequency and the low frequency non-uniformity, which means that the multi-frame accumulation class of algorithms cannot perform well. And meanwhile, the motion is mainly toward one monotonous direction, which cannot provide sufficient motion information to the algorithms using the registration method as the core.

In most cases, the infrared thermal imager is used to detect and track targets from a distance away for both civil and military aim. According to this usage, the aerophotographic image sequence captured by the thermal imager always has two main defects: 1. The scene will transfer from one to another rapidly, which means that the original correction coefficient will not be effective perfectly anymore, then the non-uniformity will show up. This will degrade the vision effort for the user. 2. During the transition, the direction of the scene motion always towards a monotonous direction, and the transfer speed may be varying from slow to fast or the opposite according to the target's movement. When these happen, if the newly non-uniformity level is too strong, the registration algorithm will stop working because no displacement can be calculated. On the other hand, if we use the multi-frame accumulation class of algorithms, the ghost artifacts will be due to occur because of the transition speed.

In the real IR detector, the high frequency non-uniformity is mostly expressed as the column or the row stripes and the low frequency non-uniformity is mostly expressed as the patchy pattern. They both exist in the image. In this paper, we mainly use a new registration method to correct them. Before we descript the algorithm, let us lay the eyes on the scope of application of our system. The IR imager is located in the mid-air by plane to capture the aerophoto of the ground. Under this particular situation, the captured image sequence will have the two defects mentioned above. Meanwhile, the second defect is more obvious. Usually the plane is flying towards a monotonous direction which means that the image sequence will move in the same direction and only this direction, a little vacillation will occur due to the bumps during the flight.

Under this consideration, we propose a novel scene-based non-uniformity correction technology not only fits the situation mentioned above but also has been realized on the small packaged, low power consumed real time hardware system. Now, the technology has been applied on a specific system for some particular usage. We test the performance of our algorithm by real captured image sequence through the hardware system.

This paper is arranged as follows. In Section 1, the space projection estimator and temporal iteration NUC algorithm is presented. The kernel idea of these two algorithms is to reduce the calculation amount and improve the convergence speed with almost no ghosting. Performance analysis of the algorithm and the effort on the real hardware system is shown in Section 2. We discuss the correction effect of our algorithm and also demonstrate the real time correction performance within the hardware platform. In Section 3, we make a conclusion and perspective of our research work.

1 Description of the space projection estimator and temporal iteration NUC algorithm

It is well known that, the non-uniformity correction is always being done by iterating the gain and bias coefficient. Since our aim is to develop an algorithm which can be fully immigrated into the FPGA based hardware system, the traditional 2-D registration is no longer applicable because it is impossible to conduct the tremendous calculation of the 2-D Fourier Transform of an image in the FPGA. We follow the inspiration of Stephen C. Cain[22] by developing a new space projection estimator to simply compute the relative displacement of two neighboring images for the registration, and then by adding a certain criterion we finish the correction. Here we describe our new space projection estimator and the adding criterion as follows:

1). If the dimension of the image is $M \times N$, the horizontal and vertical directions projections of the image, $p_x^i(i)$ and $p_x^j(i)$, can be defined respectively by:

$$p_x^i(i) \triangleq \sum_{j=1}^{N} p_x(i,j) - \sum_{i=1,j=1}^{i=M,j=N} \mathrm{Pixel}(i,j)/N \quad ,(1)$$

$$p_x^i(j) \triangleq \sum_{i=1}^{M} p_x(i,j) - \sum_{i=1,j=1}^{i=M,j=N} \mathrm{Pixel}(i,j)/M \quad .(2)$$

2). In any real imaging system, there will be new information entering the field of view. The space projection estimator is sensitive to this new information which causes the registration to be less valid. Stephen C. Cain designed a sliding window filter and added it to the space projection estimator to make the algorithm ignoring the new information. We find that the computation of this filter is still too much for the FPGA and it is hard to realize only using the Hardware Description Language (HDL). In this case, we use a cosine-sine fixed window filter as a

substitution. It turns out that, the performance of our filter is more stable than the sliding window filter, and more importantly, it is realizable. The cosine-sine fixed window filter can be described as follows.

For column projection:

$$p_x^i(j) = \begin{cases} p_x^i(j)\left(\dfrac{1+\cos(\pi(\delta_{\text{row}}-1-j)/\delta_{\text{row}})}{2}\right), j < \delta_{\text{row}} \\ p_x^i(j)\left(\dfrac{1-\sin(\pi(\delta_{\text{row}}-1-j)/\delta_{\text{row}})}{2}\right), j > N-\delta_{\text{row}} \end{cases}, \quad (3)$$

For row projection:

$$p_x^j(i) = \begin{cases} p_x^j(i)\left(\dfrac{1+\cos(\pi(\delta_{\text{col}}-1-i)/\delta_{\text{row}})}{2}\right), i < \delta_{\text{col}} \\ p_x^j(i)\left(\dfrac{1-\sin(\pi(\delta_{\text{col}}-1-i)/\delta_{\text{col}})}{2}\right), i > M-\delta_{\text{col}} \end{cases}, \quad (4)$$

where δ_{row} and δ_{col} are the maximum shift of the vertical and horizontal direction.

3). We need the two neighboring frames to determine the relative displacement. That is to say, we have to acquire two frames and set one of them as the reference frame and the other as the current frame. We use their space projection estimators to calculate the cross-correlation matrixes as follows:

$$Cof_{\text{row}} = \sum_{\substack{i=1,j=1 \\ j=N-2\delta_{\text{row}}+1}}^{i=2\delta_{\text{row}}+1} (\text{ref}_{\text{row}}(j+i-1) - \text{cur}_{\text{row}}(\delta_{\text{row}}+i))^2, \quad (5)$$

$$Cof_{\text{col}} = \sum_{\substack{i=1,j=1 \\ j=N-2\delta_{\text{col}}+1}}^{i=2\delta_{\text{col}}+1} (\text{ref}_{\text{col}}(j+i-1) - \text{cur}_{\text{col}}(\delta_{\text{col}}+i))^2. \quad (6)$$

Once the cross-correlation matrixes have been determined, we can get the relative displacement d_{row} and d_{col} by choosing the minimum value among these two matrixes:

$$d_{\text{row}} \triangleq \arg\min(\text{Cof}_{\text{row}}), \quad (7)$$

$$d_{\text{col}} \triangleq \arg\min(\text{Cof}_{\text{col}}). \quad (8)$$

After the registration, we discuss the certain criterion used as the implementation of the correction. We use a 3×3 window to conduct the criterion by comparing the 4 neighboring pixel value to the center pixel to adjust the original image as follows:

$$\begin{cases} P_{adj}^{(i,j-1)} = |P(i,j-1) - P(i,j)| < \text{TH} \\ P_{adj}^{(i,j+1)} = |P(i,j+1) - P(i,j)| < \text{TH} \\ P_{adj}^{(i-1,j)} = |P(i-1,j) - P(i,j)| < \text{TH} \\ P_{adj}^{(i+1,j)} = |P(i+1,j) - P(i,j)| < \text{TH} \end{cases}. \quad (9)$$

Usually the 2-D registration algorithm will conduct the correction on both the gain and bias coefficient after the relative displacement has been computed. But our algorithm divides the correction into two parts as shown above especially for the scope of application of our aerophotographic image sequence. The learning rate has been divided into both the registration part and the criterion part. It can be seen from the equations, the criterion we used will work together with the space projection estimator to conduct the correction. To the real image sequence, the space projection estimator will be affected by the high frequency non-uniformity and cause it to work less effectively. The criterion we used to converge the high frequency non-uniformity is faster than the low frequency non-uniformity. Once the high frequency non-uniformity has been weakened, the space projection estimator will calculate the relative displacement of neighboring frames accurately. Then the low frequency non-uniformity will be corrected after several frames.

The next image sequence is captured using our hardware system with this proposed technology. We locate the IR imager on a plane while it is flying across the city. This makes the image sequence moving towards a monotonous direction of the south. And it can be seen from the sequence that the image has stripe pattern high frequency non-uniformity and the patchy pattern low frequency non-uniformity. In fact, in most of the real application of the imager, the non-uniformity pattern will have both these two kinds and the similar motion. When the algorithm starts working, the incoming image will first be adjusted by the criterion of Eq. (10). Then the algorithm will calculate the error $E_{\text{criterion}}(i,j)$ between the original image and the adjusted image, and use the error to conduct the convergence one time as follows:

$$E_{\text{criterion}}(i,j) = P(i,j) - p_{\text{out}}(i,j), \quad (11)$$

$$\text{Gain}(i,j) = \begin{cases} \text{Gain}_{\text{xoriginal}}(i,j) + \alpha_{\text{criterion}} \cdot E_{\text{criterion}}(i,j)Y(i,j) \\ \text{where}(i,j)\text{th is in the overlap area} \\ \text{Gain}_{\text{original}}(i,j) \quad \text{else} \end{cases}, \quad (12)$$

$$\text{Offset}(i,j) = \begin{cases} \text{Offset}_{\text{original}}(i,j) + \alpha_{\text{criterion}} \cdot \text{ERROR}_{\text{criterion}}(i,j) \\ \text{where}(i,j)\text{th is in the overlap area} \\ \text{Offset}_{\text{original}}(i,j) \quad \text{else} \end{cases}, \quad (13)$$

where the $\text{Gain}(i,j)$ and $\text{Offset}(i,j)$ are the corrected coefficient under the criterion, $\alpha_{\text{criterion}}$ is the learning rate under the criterion, $Y(i,j)$ is the observed signal of the FPA.

As we mentioned above, the criterion is effective to the high frequency non-uniformity. After the one time convergence, the space projection estimator will step up to calculate the overlap area of neighboring frames to determine the relative displacement, thus to conduct the second time convergence as follows[20]:

$$e_n(i,j) = X_{n-1}(i-d_{\text{row}}, j-d_{\text{col}}) - X_n(i,j), \quad (14)$$

$$\text{Gain}_{n+1}(i,j) = \begin{cases} \text{Gain}_n(i,j) + \alpha_{PE} \cdot e_n(i,j)Y_n(i,j) \\ \text{where}(i,j)\text{th is in the overlap area} \\ \text{Gain}_n(i,j) \quad \text{else} \end{cases}, \quad (15)$$

$$\text{Offset}_{n+1}(i,j) = \begin{cases} \text{Offset}_n(i,j) + \alpha_{PE} \cdot e_n(i,j) \\ \text{where}(i,j)\text{th is in the overlap area} \\ \text{Offset}_n(i,j) \quad \text{else} \end{cases}, \quad (16)$$

where the $e_n(i,j)$ is error matrix of the neighboring

$$\begin{cases} P_{\text{out}}(i,j) = P(i,j); P_{adj}^{(i,j-1)} + P_{adj}^{(i,j+1)} + P_{adj}^{(i-1,j)} + P_{adj}^{(i+1,j)} = 0 \\ P_{\text{out}}(i,j) = \dfrac{P_{adj}^{(i,j-1)} \cdot P(i,j-1) + P_{adj}^{(i,j+1)} \cdot P(i,j+1) + P_{adj}^{(i-1,j)} \cdot P(i-1,j) + P_{adj}^{(i+1,j)} \cdot P(i+1,j)}{P_{adj}^{(i,j-1)} + P_{adj}^{(i,j+1)} + P_{adj}^{(i-1,j)} + P_{adj}^{(i+1,j)}}; \text{else.} \end{cases} \quad (10)$$

frames. The $\mathrm{Gain}(i,j)$ and $\mathrm{Offset}_n(i,j)$ are the corrected coefficient under the space projection estimator. α_{PE} is the learning rate under the space projection estimator. These are the accelerations in spatial-domain.

To get more accurate estimate and fast convergence, we iterate the $\mathrm{Gain}_n(i,j)$ and $\mathrm{Offset}_n(i,j)$ parameter in K adjacent frames, which can be regarded as the acceleration in time-domain.

For $k \in [0, K-1]$

For $l \in [k, K-1]$

$$E_{n,l}(i,j) = X_{n-l}(i,j) - X_{n-l-1}(i+h, j+v)$$

$$\mathrm{Gain}_{n,l}(i,j) = \begin{cases} \mathrm{Gain}_{n-l-1}(i,j) + \alpha \cdot E_{n,l}(i,j) Y_{n,l}(i,j) \\ \text{where } (i,j) \text{ th is in the overlap area} \\ \mathrm{Gain}_{n-l-1}(i,j) \quad \text{else} \end{cases}$$

$$\mathrm{Offset}_{n,l}(i,j) = \begin{cases} \mathrm{Offset}_{n-l-1}(i,j) + \alpha \cdot E_{n,l}(i,j) \\ \text{where } (i,j) \text{ th is in the overlap area} \\ \mathrm{Offset}_{n-l-1}(i,j) \quad \text{else} \end{cases} \quad . (17)$$

So the total number of iteration is $K \cdot (K-1)/2$. The use of correlation of adjacent frames, together with iteration strategy between them, makes our algorithm's convergence speed so high that processed images have almost no ghosting artifacts.

2 Performance analysis of the algorithm and the effort on the real hardware system

In this section, we will analyze the performance of our algorithm by some evaluation indexes, and then demonstrate the real effort of this technology by applying it onto a real time FPGA based hardware system.

The following figure is captured by the hardware system using an EP2C20 serious FPGA as the processing unit:

It can be seen from Fig. 1 that the captured image has strong stripe pattern high frequency non-uniformity and patchy pattern low frequency non-uniformity. The convergence step just like what we have discussed above. To compare with the traditional 2-D registration algorithm, we process both our technology and the traditional 2-D registration algorithm on the same image sequence. As we predicted before, if we only conduct the traditional 2-D registration algorithm, it is hard for us to find the exact movement of the sequence, which makes the algorithm think the image sequence is zero moving.

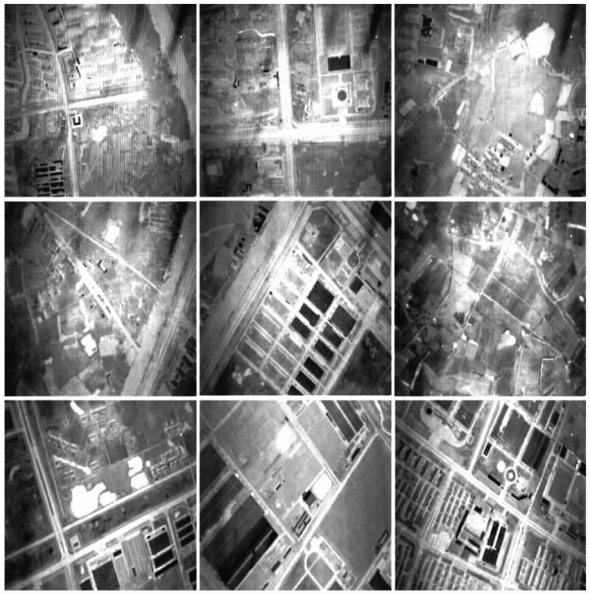

Fig. 1　The real performance on the hardware system
图 1　硬件系统的实时性能效果图

After a few frames, the stripe pattern high frequency non-uniformity has been corrected, leaving only the patchy pattern low frequency non-uniformity. Then the projection estimator can work its magic and finally correct most of the patchy pattern low frequency non-uniformity. Finally, the iteration method is used to get more accurate estimate and fast convergence.

The following experiment is designed for comparing the proposed method with the GALMS method[13] and the TV method[23]. The infrared sequence with artificial non-uniformity is generated from a clear 300 frames infrared video sequence acquired at 50 frames per second (FPS), using a synthetic gain with a unit-mean Gaussian distribution with standard deviation of 0.2, and a synthetic offset with a zero-mean Gaussian distribution with standard deviation of 40. The metric used to measure the NUC performance is given by the root-mean-square error (RMSE), which is defined as

$$\mathrm{RMSE} = \sqrt{\frac{1}{MN}\sum_{i,j}\left(X(i,j) - \hat{X}(i,j)\right)^2} \quad , \quad (18)$$

where $X(i,j)$ is the original value of the pixel, $\hat{X}(i,j))$ is the corrected value of the pixel. M、N is the dimension of the image.

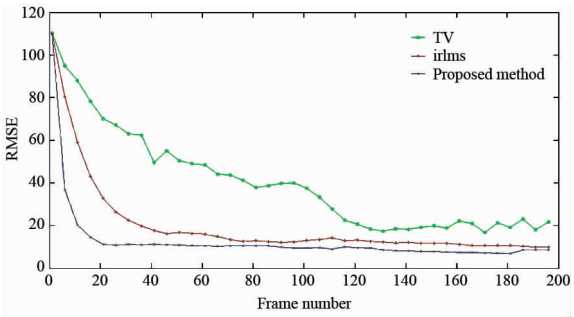

Fig. 2　RMSE results of the non-uniformity correction using different methods
图 2　多种非均匀性校正方法的 RMSE 测试图

It can be observed from Fig. 2 that the RMSE of the proposed method can be reduced below 20 within only 20 frames, when the criterion is dealing with the high frequency non-uniformity. Then the convergence speed is slowing down because the low frequency non-uniformity is being corrected. As mentioned above, the speed is also involved with the learning rate. During the test, we choose the two learning rates as 0.03 both.

Figure 3 shows the images for the 20th frame. Figure 3(a) shows the raw image corrupted with simulated non-uniformity. The outputs using GALMS, TV and SPETI are shown in Figs. 3(b)-3(d), respectively.

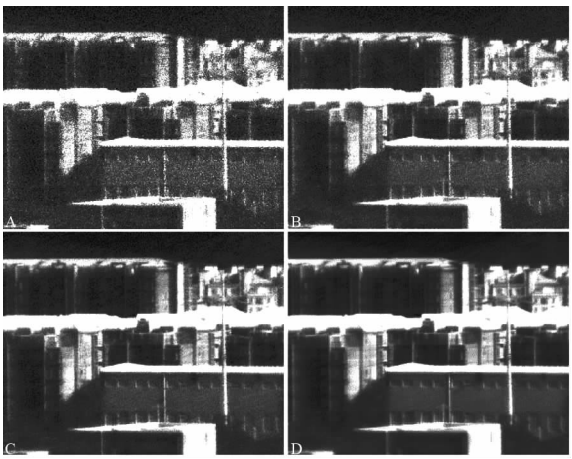

Fig. 3 Correction with simulated non-uniformity images using different methods(Frames 20th) (a) Images with simulated gain and offset non-uniformity, (b) Corrected result of the GALMS method, (c) Corrected result of the TV method, (d) Corrected result of the proposed method

图3 多种模拟非均匀性校正算法效果图(第20帧)(a)添加模拟增益和偏置的非均匀性图像,(b)GALMS算法校正效果图,(c)TV算法校正效果图,(d)本文算法校正效果图

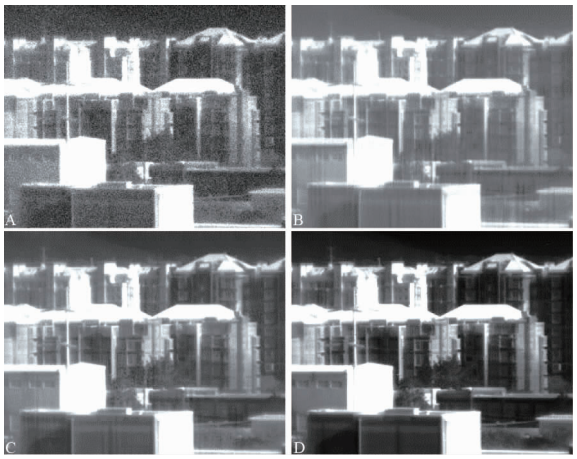

Fig. 4 Correction with simulated non-uniformity images using different methods(Frames 410th) (a) Images with simulated gain and offset non-uniformity, (b) Corrected result of the GALMS method, (c) Corrected result of the TV method, (d) Corrected result of the proposed method

图4 多种模拟非均匀性校正算法效果图(第410帧)(a)添加模拟增益和偏置的非均匀性图像,(b)GALMS算法校正效果图,(c)TV算法校正效果图,(d)本文算法校正效果图

The GALMS method, in contrast, converges more slowly. There is still heavy non-uniformity in the outputs of GALMS. The TV method converges much faster than the GALMS, but there is still some residual non-uniformity that can be perceived in the outputs of TV. However, in the SPETI's output, it effectively generates much fewer ghosting artifacts than the other techniques. Besides, the level of residual non-uniformity is rather low. It can be seen that the proposed SPETI algorithm almost eliminated the FPN within only 20 frames. It is easy to find that the SPETI compensates the non-uniformity the fastest and performs the best over the sequence.

After dozens of frames, the non-uniformity level of the GALMS and TV method has been lowered to an acceptable level, kind of like the final result shown in Fig. 4(b)-4(c). The result of GALMS shows serious ghosting, while some ghosting artifacts of the wire poles can be appreciated in the result of TV. At the same time, there is almost no ghosting artifact in the result of SPETI. It is no wonder that SPETI gives good results.

3 Conclusion

In this paper, we propose a new scene-based non-uniformity correction technology for the monotonous motion and complex non-uniformity. Our technology is more effective than the multi-frame accumulation class of algorithms, and meanwhile, comparing to the traditional 2-D registration algorithm, our algorithm is much simpler in computation according to its theory and can be fully realized on the hardware system with only one FPGA as the core and no report shows that the 2-D traditional registration algorithm can do the same thing. We finish the immigration and use the system we build to test the performance of our technology. Somehow there are still some defects existing in the algorithm, for example in Fig. 1, there is still some left over low frequency non-uniformity. This is because the motion of the image sequence is almost extremely towards a monotonous direction, which makes the brightness of that area hard to transfer into the next frame. We will continue our research and fix this problem in the future work.

Acknowledgement

This project is supported by the Natural Science Foundation of Jiangsu Province of China, under Grant No. BK20130769.

References

[1] Scribner D A, Kruer M, Killiany J. Infrared focal planearray technology[J]. *Proc. IEEE*, 1991, **79**: 66-85.

[2] Ratliff B M, Hayat M M, Tyo J S. Generalized algebraic scene-based nonuniformity correction algorithm[J]. *Opt. Soc. Am. A*, 2005, **22**: 239-250.

[3] Harris J G, Chiang Y M. Minimuzing the 'ghosting' artifact in scene-based nonuniformity correction[J], *SPIE*, 1998, **3377**: 106-113.

[4] Harris J G, Chiang Y M. Nonuniformity correction of infrared image sequences using the constant-statistics constraint[J], *IEEE*, 1999, **8**: 1148-1151.

[5] Harris J G, Chiang Y M. Nonuniformity correction using the constant-statistics constraint: analog and digital implementations[J]. *SPIE*, 1997, **3061**: 895-905.

[6] Hayat M M, Torres S N, Armstrong E E, *et al*. Statistical algorithm for non-uniformity correction in focal-plane arrays[J]. *App. Opt*, 1999, **38**: 772-780.

[7] Ratliff B M, Hayat M M. An algebraic algorithm for nonuniformity correction in focal-plane arrays[J]. *Opt. Soc. Am*, 2002, **19**: 1737-1747.

[8] Ratliff B M, Hayat M M, Tyo J S. Radiometrically accurate scene-based nonuniformity correction for array sensors[J]. *Opt. Soc. Am. A*, 2003, **20**: 1890-1899.

[9] Scribner D, Sarkady K, Caulfield J, *et al*. Non-uniformity correction

for staring focal planearrays using scene-based techniques[J]. *Proc. SPIE*, 1990, **1308**: 224 - 233.

[10] Scribner D, Sarkady K, Kruer M, *et al*. Adaptive nonuniformity correction for IR focal plane arrays using neural networks[J]. *Proc. SPIE*, 1991, **1541**: 100 - 109.

[11] Torres S N, Hayat M M. Kalman filtering for adaptivenonuniformity correction in infrared focal plane arrays[J]. *Opt. Soc. Am. A*, 2003, **20**: 470 - 480.

[12] Torres S N, Pezoa J E, Hayat M M. Scene-based nonuniformity correction for focal plane arrays by the method of the inverse covariance form[J]. *Appl. Opt.* 2003, **42**: 5872 - 5881.

[13] Hardie R, Baxley F, Brys B, *et al*. Scene-based nonuniformity correction with reduced ghosting using a gated LMS algorithm[J]. *Opt. Express*, 2009, **17**: 14918 - 14933.

[14] Hardie R C, Hayat M M, Armstrong E E, *et al*. Scene-based nonuniformity correction using video sequences and registration[J]. *Appl. Opt*. 2000, **39**: 1241 - 1250.

[15] Zuo C, Chen Q, Gu G, *et al*. Registration method for infrared images under conditions of fixed-pattern noise[J]. *Opt Commun*, 2012, **285**: 2293 - 2302.

[16] Zuo C, Chen Q, Gu G H, *et al*. Scene-based nonuniformity correction algorithm based on interframe registration[J]. *Opt Soc Am A*, 2011, **28**: 1164 - 1176.

[17] Zuo C, Chen Q, Gu G, *et al*. New temporal high-pass filter nonuniformity correction based on bilateral filter[J]. *Opt. Rev*. 2011, **18**: 197 - 202.

[18] Qian W X, Chen Q, Gu G H. Space low-pass and temporal high-pass nonuniformity correction algorithm[J]. *Opt. Rev*, 2010, **17**: 24 - 29.

[19] Qian W X, Chen Q, Gu G H. Minimun mean square error method for stripe nonuniformity correction[J]. *Chin Opt Lett*, 2011, **051103**: 1 - 3.

[20] Qian W H, Chen Q, Bai J Q, *et al*. Adaptive convergence nonuniformity correction algorithm[J]. *App Opt*, 2011, **50**: 1 - 10.

[21] Harris J, Chiang Y. Minimizing the 'ghosting' artifact in scene-based nonuniformity correction[J]. *Proc. SPIE*, 1998, **3377**:106 - 113.

[22] Cain S C, Hayat M M, Armstrong E E. Projection-based image registration in the presence of fixed-pattern noise[J]. *IEEE*, 2001, **10**: 1860 - 1872.

[23] Esteban V, Pablo M, Sergio T. Total variation approach for adaptive nonuniformity correction in focal-plane arrays[J]. *Optics Letters*, 2011, **36**: 172 - 174.